American Mineralogist, Volume 76, pages 332–342, 1991

Substructure and superstructure of mullite by neutron diffraction

R. J. Angel
Department of Geological Sciences, University College London, Gower Street, London WC1E 6BT, England,
and Department of Crystallography, Birkbeck College, Malet Street, London WC1E 7HX, England
R. K. McMullan
Department of Chemistry, Brookhaven National Laboratory, Upton, New York 11973, U.S.A.
C. T. Prewitt
Geophysical Laboratory, Carnegie Institution of Washington, 5251 Broad Branch Road NW, Washington, DC 20015-1305, U.S.A.

Abstract

The average structure of mullite with approximate composition $SiO_2 \cdot 2Al_2O_3$ has been refined using single-crystal neutron diffraction data. A split-site model for both tetrahedral and O positions was refined in order to reflect the local structural variation arising from both O-vacancy and Al-Si ordering. The resulting local atomic configurations are similar to those found in the related, but commensurate, phases sillimanite (Al_2SiO_5) and $Al_5(BO_3)O_6$. The intensities of satellite reflections at positions $\frac{1}{2}\mathbf{c}^* \pm q\mathbf{a}^*$, where $q \approx 0.30$ were also measured using single-crystal neutron diffraction. Analysis by Patterson methods demonstrates that these satellites arise from an incommensurate modulation involving two ordering patterns. The difference structures corresponding to these ordering patterns have symmetries P_cnnm and P_cbnm. Both require ordering of Al and Si over the tetrahedral sites within the mullite structure, and the P_cnnm ordering also includes the ordering of O atoms and vacancies on one O atom site, which also drives Al ordering between the T and T* tetrahedral sites. The results demonstrate that the mullite structure is very well ordered on a local scale, with a corresponding low configurational entropy.

Introduction

The characterization of the state of order of a crystalline substance is necessary to complete its thermodynamic description. For example, changes in the ordering of Al and Si can have profound effects on the entropy and enthalpy of aluminosilicates. Many stoichiometric minerals undergo simple order-disorder transitions that are relatively well understood. However, when the phase is a solid solution and, therefore, of variable stoichiometry, a simple ordering pattern may not exist. Many solid solutions unmix at low temperatures into either the stoichiometric ordered end-members, or two phases of intermediate composition that are able to develop simple ordering patterns. A third type of behavior is exhibited by several important minerals, including plagioclase feldspars and mullite. In these phases, intermediate compositions contain ordering patterns that are modulated through the structure with repeat periods that are not, in general, a simple multiple of the periodicity of the underlying lattice. Such phases are termed incommensurate, and it is the purpose of this paper to demonstrate that such structures are indeed very well ordered.

Heine and McConnell (1984) showed that the phase transition in insulators from a high-temperature disordered phase to a low-temperature incommensurately ordered phase may be described in terms of a substructure overlain by an incommensurate superstructure. The scattering density within the incommensurate crystal may then be written as

$$\rho(\mathbf{l} + \mathbf{r}) = \rho_{ave}(\mathbf{r}) + \rho_1(\mathbf{r})\cos \mathbf{q}\cdot\mathbf{l} + \rho_2(\mathbf{r})\sin \mathbf{q}\cdot\mathbf{l} \quad (1)$$

where $\mathbf{r}$ is the position vector within a unit cell. The term $\rho_{ave}(\mathbf{r})$ is the part of the scattering density that is identical in every unit cell of the structure and is therefore the underlying substructure or average structure of the material. The two ordering schemes required by theory are represented by the difference structures $\rho_1(\mathbf{r})$ and $\rho_2(\mathbf{r})$, and these are modulated in quadrature through the structure by the sine and cosine terms, which include the wave vector of the modulation, $\mathbf{q}$, and the lattice vector of each unit cell, $\mathbf{l}$. These two difference structures are commensurate in themselves, so the analysis of the satellite diffraction intensities arising from these ordering schemes does not require the use of arbitrary supercells along the wave vector of the modulation, as the incommensurate nature of the structure is accounted for by the sine and cosine terms in Equation 1. Further discussion of the physics underlying this analysis may be found in Heine and McConnell (1984).

Fourier inversion of Equation 1 to obtain the diffracted intensities from an incommensurate crystal requires that phase factors $\mathbf{q}\cdot\mathbf{l}$ be replaced by continuous phase factors $\mathbf{q}\cdot(\mathbf{l} + \mathbf{r})$:

0003–004X/91/0304–0332$02.00

$$\rho(\mathbf{l} + \mathbf{r}) = \rho_{ave}(\mathbf{r}) + \rho'_1(\mathbf{r})\cos \mathbf{q}\cdot(\mathbf{l} + \mathbf{r}) + \rho'_2(\mathbf{r})\sin \mathbf{q}\cdot(\mathbf{l} + \mathbf{r}). \quad (2)$$

The $\rho_{ave}(\mathbf{r})$ is then the structure obtained by refinement using the Bragg diffraction intensity alone, whereas the two difference structures $\rho'_1(\mathbf{r})$ and $\rho'_2(\mathbf{r})$, not the same as $\rho_1(\mathbf{r})$ and $\rho_2(\mathbf{r})$, contribute only to the intensities of the satellites. Either description of the modulated structure is formally correct (McConnell and Heine, 1984), but one or the other may be more useful in obtaining a physical picture of the atomic arrangements within the crystal. When there is no correlation between the occupancies and the positions of different atomic sites, the ordering schemes $\rho'_1(\mathbf{r})$ and $\rho'_2(\mathbf{r})$, obtained directly by Fourier inversion of the satellite intensities, are the appropriate description. However, if crystal chemical considerations require that the same phase factor applies to an extended group or cluster of atoms, the local arrangements of atoms (i.e., occupancies and positions) are then described by $\rho_1(\mathbf{r})$ and $\rho_2(\mathbf{r})$, obtained from $\rho'_1(\mathbf{r})$ and $\rho'_2(\mathbf{r})$ by

$$\rho_1(\mathbf{r}) = \rho'_1(\mathbf{r})\cos \mathbf{q}\cdot\mathbf{r} + \rho'_2(\mathbf{r})\sin \mathbf{q}\cdot\mathbf{r}$$
$$\rho_2(\mathbf{r}) = \rho'_2(\mathbf{r})\cos \mathbf{q}\cdot\mathbf{r} - \rho'_1(\mathbf{r})\sin \mathbf{q}\cdot\mathbf{r}. \quad (3)$$

The first application of the methods outlined by McConnell and Heine (1984, 1985b) to the analysis of an incommensurate structure was to X-ray diffraction data collected from mullite (Angel and Prewitt, 1986, 1987). In brief, the average structure was obtained by conventional refinement using only Bragg diffraction data, and the satellite diffraction intensities were analyzed separately by the construction of plus and minus difference Patterson functions (McConnell and Heine, 1984) from which the two difference structures were derived. Despite the general success of this work, some uncertainties regarding the details of the ordering patterns remained because of the difficulty of distinguishing between Al and Si with X-ray diffraction data. Furthermore, the ordering patterns reported by Angel and Prewitt (1987) corresponded to those of Equation 2, whereas, because tetrahedral site occupancies and the displacements of other O atoms must be correlated with O-vacancy ordering on the Oc of the mullite structure (e.g., Burnham, 1964; Ylä-Jääski and Nissen, 1983; Angel and Prewitt, 1987; Welberry and Withers, 1990), the correct interpretation of the incommensurate ordering in mullite should be based upon ordering schemes of the type described in Equation 1.

We have therefore undertaken a neutron diffraction study of mullite with the intention of resolving the question of Al-Si distribution within the structure and correcting any erroneous conclusions that may have arisen from the use of the inappropriate interpretation of the ordering schemes in the previous analysis by Angel and Prewitt (1987). Following the methodology implied by both Equations 1 and 2, we describe the average structure of mullite refined using Bragg neutron diffraction data measured with a large single crystal. This average structure includes several partially occupied sites. The local arrangement of atoms within the structure is deduced from the average structure by applying crystal chemical reasoning and by comparing the average structure with the known structures of two closely related, stoichiometric ordered structures. The arrangement of these local clusters within the crystal is given by the difference structures $\rho_1(\mathbf{r})$ and $\rho_2(\mathbf{r})$, and, we show, by use of Patterson functions, that only certain ordering patterns are compatible with the observed satellite intensity data. Given the equivalence (Simmons and Heine, 1987) of this analysis of incommensurate structures with the superspace group approach (e.g., de Wolff et al., 1981), these results should provide the starting point for a suitable four-dimensional refinement.

Experimental

The mullite crystal used in this study was from the sample denoted by Cameron (1977) as no. 5, a portion of which was used for the X-ray studies reported by Angel and Prewitt (1986, 1987). The analysis reported by Cameron (1977) indicates that the crystal contains less than 0.02 wt% TiO_2 and approximately 0.1 wt% Fe_2O_3 and has a composition corresponding to $x = 0.40(1)$ in the formula $Al_2[Al_{2+2x}Si_{2-2x}]O_{10-x}$. The satellite diffraction peaks in this sample are significantly less sharp than the Bragg reflections and correspond to maxima in the complex diffuse scattering from this particular sample (Welberry and Withers, 1990). However, this was the only sample available in sufficiently large single crystals to enable us to carry out neutron diffraction studies, and we believe that the results obtained are generally applicable to other members of the mullite solid solution that display sharp satellite diffraction maxima. A single crystal of approximate volume 13 mm^3 (Table 1) was used to measure satellite intensity data, but because of severe extinction effects on the Bragg reflections, a smaller fragment, 1.08 mm^3 in volume, cut from this crystal was used to measure the Bragg diffraction data.

Neutron diffraction data were measured with an automated four-circle diffractometer on beam line H6 of the high flux beam reactor at Brookhaven National Laboratory. A neutron beam was obtained from the 002 reflection of a Be monochromator. The wavelength of 1.0353(1) Å was determined by a least-squares fit of $\sin^2\theta$ data for a KBr reference crystal [$a = 6.60000(13)$ Å at 25 °C]. Lattice parameters of mullite were determined by a least-squares fit of $\sin^2\theta$ data for 32 reflections. These differ significantly from those determined in the previous X-ray experiments (Table 1), a difference we attribute to the poorer peak profiles obtained from the crystal used in this study. All bond lengths and angles reported in this paper were therefore calculated with the X-ray cell parameters.

Intensity data were measured with $\theta/2\theta$ step scans, with the counts at each step accumulated for a preset number of monitor counts of the direct beam. Fixed scan widths in 2θ were used for reflections with $\sin\theta/\lambda < 0.45$ Å^{-1}, and variable scan widths calculated from an empirical dispersion relationship were used for reflections with $\sin\theta/\lambda > 0.45$ Å^{-1}. The intensities of two standard reflec-

TABLE 1. Crystallographic data for mullite

A:	**Unit-cell data**	**Present work**	**X-ray***
	λ (Å)	1.0353(1)	Mo$K\alpha$
	a (Å)	7.588(2)	7.5785(6)
	b (Å)	7.688(2)	7.6817(7)
	c (Å)	2.8895(6)	2.8864(3)
B:	**Description of crystal**	**Bragg**	**Satellites**
	Max dimensions (mm)	1.2 × 1.2 × 1.5	1.6 × 1.7 × 5.3
	Volume by calculation (mm³)	1.08	13.2
	Absorption coefficient (cm⁻¹)	0.0041	0.0041
C:	**Data collection**		
	Temperature (°C)	24	24
	$\sin\theta_{max}/\lambda$(Å⁻¹)	0.796	0.683
	Scan width (° in 2θ)	3.0–5.0	3.0–5.0
	Steps per scan	75–95	75-95
	No. reflections	709 (2 octants)	456 (1 octant)
D:	**Refinement using Bragg data**	**Model 1**	**Model 2**
	No. observations (*No*)	709	709
	No. parameters (*Np*)	46	46
	$R_u(F)$	3.7%	3.7%
	$R_w(F)$	4.5%	4.5%
	Goodness of fit	1.61	1.62
	$\lvert F_o - F_c\rvert_{max}/\sigma_F$	7.2 (24$\bar{1}$)	7.0 (24$\bar{1}$)
	Max. extinction factor	0.28 (002)	0.28 (002)
	Mosaic spread (secs of arc)	0.52, 0.21, 0.13	0.54, 0.20, 0.15
	$\lvert\Delta\rho_{max}\rvert/\rho$	1.3%	0.8%

Note: Figures in parentheses represent estimated standard deviations in the last decimal place quoted. This convention applies to all subsequent tables.

* X-ray cell parameters from Angel and Prewitt (1986).

tions were monitored at regular intervals, and they showed no significant variation with time. The step scans of the Bragg reflections were integrated with a modified Lehmann-Larsen algorithm (Grant and Gabe, 1978) with the option to modify background settings interactively. Satellite intensity data were integrated by taking the first and last 10% of each scan as representative of the background and then subtracting the calculated background from the counts accumulated for the central 80% of the scan.

Refinements using the Bragg reflection data were carried out with the RFINE-88 program, a development version of RFINE-4 (Finger and Prince, 1975). All refinements utilized F with weights set to $[\sigma_F^2 + (0.02F)^2]^{-1}$, where σ_F was derived from counting statistics. Five reflections with $I < 0$ were included in the refinements with F set to zero. Neutron scattering lengths of $5.803f$ (= fermi) for O, $3.449f$ for Al, and $4.149f$ for Si were taken from Koester and Steyerl (1977). The atomic parameters reported by Angel and Prewitt (1986) were taken as starting values in the refinements, the results of which are discussed in detail below. Initial refinements resulted in many strong reflections exhibiting $F_{obs} < F_{calc}$, a clear indication of the presence of extinction effects. A correction for isotropic secondary extinction reduced the magnitude of $F_{obs} - F_{calc}$ for many of these reflections but failed to correct the observed variation in ψ-scan data. The introduction of anisotropic extinction parameters (type I crystal with Lorentzian mosaic distribution; Becker and Coppens, 1974) reduced the discrepancies for the strongest reflections (002 and 00$\bar{2}$) from $(F_{obs} - F_{calc})/\sigma_F = -111$ to -2 and R_u from 4.3 to 3.7%, as well as corrected the ψ-scan data. The presence of anisotropic extinction precluded the averaging of the data, so all of the refinements reported here were for two asymmetric units of unaveraged data and include a refined anisotropic extinction correction.

AVERAGE STRUCTURE

The mullite structure consists of chains of edge-sharing AlO_6 octahedra parallel to the **c** axis. These octahedral chains are cross-linked by double chains of Si and Al tetrahedra in an arrangement that is similar to that found in sillimanite (Fig. 1A). In mullite, however, the ratio of tetrahedral Al:Si is greater than the ratio 1:1 found in sillimanite, and some O sites are only partially occupied so as to compensate for the substitution of Al for Si:

$$2^{[4]}Si^{4+} + O^{2-} \rightarrow 2^{[4]}Al^{3+} + \square. \quad (4)$$

This exchange reaction is the basis of the mullite solid solution $Al_2[Al_{2+2x}Si_{2-2x}]O_{10-x}$ in which x can range (in principle) from 0, which corresponds to sillimanite, Al_2SiO_5, to 1, which corresponds to Al_2O_3. The partially occupied O site in the mullite structure is Oc, which forms the central cross link in the double tetrahedral chains. When this site is vacant the coordination by O of the two adjacent T sites is only three, so these are also vacant in preference to occupancy of a pair of alternative sites denoted T*. In order to maintain reasonable tetrahedral coordination of these T* sites, the bridging O atoms of the adjacent T-O-T groups are displaced toward the T* sites to form a T_2T^*O group (Fig. 1B). This displaced O site is designated Oc*.

The average structure corresponding to this general scheme was first determined with X-ray diffraction data by Sadanaga et al. (1962) and confirmed by Burnham (1964) and Ďurovič (1969). Ďurovič and Fejdi (1976)

found essentially the same structure for a phase in which the Si was replaced by Ge, and more recently the average structure was analyzed to somewhat higher resolution by Angel and Prewitt (1986). The parameters of this average structure model were refined using our neutron diffraction data with the occupancies of all sites constrained to correspond to the composition $x = 0.40$ and all of the Si allocated to the T site. The ~18% difference between the neutron scattering lengths of Al and Si normally allows their distribution in aluminosilicates to be refined directly. A refinement of the distribution of Si and Al between the T and T* sites was therefore carried out, subject to the constraint of $x = 0.40$. This resulted in a significant improvement in the refinement indices and, also, in similar thermal parameters for the two types of tetrahedral sites. Final refinement indices, positional parameters, and bond lengths from this refinement are reported in Tables 1, 2, and 3 under model 1. The refined scattering lengths for the tetrahedral sites correspond to a distribution of 0.05(2)Si + 0.15(2)Al on T* and 0.25(2)Si + 0.55(2)Al on T, if the composition corresponds exactly to $x = 0.40$. However, the esd of 0.02 for these occupancies from the refinement does not account for the uncertainty of ±0.01 in x; when this is included the esd for the Si occupancy of both sites becomes ±0.04. A further refinement, in which x and the distribution of Si and Al were varied, gave T* = 0.065(23)Si + 0.128(24)Al, T = 0.242(23)Si + 0.565(23)Al, and $x = 0.386(6)$, although the refinement indices showed no improvement in fitting the data. We therefore conclude that the current data do not distinguish between a model with all of the Si on the T sites or one with some small amount of Si on the T* sites.

The positional parameters of model 1 (Table 2) are identical, within 3σ, to those previously reported by Burnham (1964) for an almost identical composition and to the final parameters reported for this sample by Angel and Prewitt (1987), with the exception of the Oab site. There are a number of shortcomings with this simple model. The thermal parameters of the O sites are very large compared to those of the corresponding sites in sillimanite (Peterson and McMullan, 1986). In particular, the thermal ellipsoids of the Oab and Od atoms are elongated parallel to the vector between T and T*, a result ascribed by Burnham (1964) to different positions for these atoms as correlated with the local occupancies of T or T*. Furthermore, the T-O bond lengths (Table 3) are intermediate between those of the Si and Al tetrahedra of sillimanite. This is consistent with the T site containing both Al and Si, and further O displacements associated with ordering of them are also to be expected.

Angel and Prewitt (1987) refined anharmonic thermal parameters for the Oab and Od O sites in order to model the different positions of the O atoms taken in response to different local T and T* site occupancies. The same approach was successfully applied to our neutron data, but the absence of sin θ/λ variation in neutron scattering lengths allows the more direct approach of refining split sites for several atom positions. A starting model was

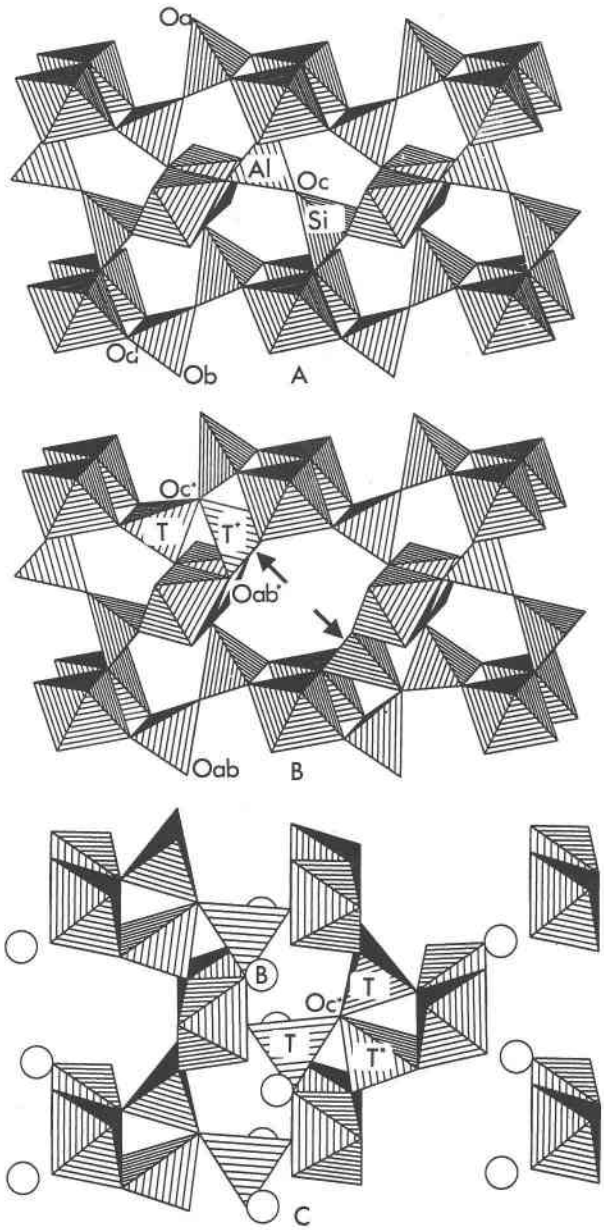

Fig. 1. (**A**) Sillimanite viewed approximately along the c axis (coordinates from Peterson and McMullan, 1986). (**B**) The local configuration around a single O vacancy in mullite. The arrows indicate the transfer of Al from the T sites adjoining the vacancy into T* sites. (**C**) A single layer of the structure of $Al_5(BO_3)O_6$, in which all of the tetrahedra are involved in T_3O groups. The site labeling follows that of mullite, not that of the original structure determination (Sokolova et al., 1978); circles represent three-coordinate B. Drawings made with a modified version of Struplo (Fischer, 1985).

developed by comparisons with the structures of sillimanite (Fig. 1A) and a boroaluminate, $Al_5(BO_3)O_6$, with a very similar structure (Fig. 1C; Sokolova et al., 1978). The AlO_6 octahedra in this structure are arranged in the same way as those in mullite and sillimanite, whereas the

TABLE 2. Positional and thermal parameters for mullite

Site	x	y	z	β_{11}	β_{22}	β_{33}	β_{12}	B_{eq}/B_{iso}	Occ.
				Model 1					
Al	0	0	0	0.0025(1)	0.0017(1)	0.0105(9)	0.0002(1)	0.45	1.0 Al
T	0.1490(1)	0.3400(1)	1/2	0.0017(1)	0.0022(1)	0.0141(9)	−0.0001(1)	0.46	**
T*	0.2625(5)	0.2067(5)	1/2	0.0017(5)	0.0021(5)	0.017(4)	−0.0001(4)	0.48	**
Oab	0.35838(7)	0.42238(8)	1/2	0.0044(1)	0.0062(1)	0.0111(6)	−0.00285(6)	0.95	1.0 O
Oc	1/2	0	1/2	0.0052(6)	0.0050(6)	0.062(3)	−0.0013(4)	1.48	0.4 O
Oc*	0.4495(5)	0.0509(5)	1/2	0.0026(6)	0.0023(6)	0.028(3)	−0.0003(3)	0.69	0.2 O
Od	0.12733(7)	0.21843(7)	0	0.0049(1)	0.0041(1)	0.0258(7)	−0.00232(5)	0.98	1.0 O
				Model 2					
Al	0	0	0	0.0024(1)	0.0017(1)	0.0102(9)	0.0002(1)	0.43	1.0 Al
T1	0.148(1)	0.3455(9)	1/2					0.43(2)	0.3 Si
T2	0.1502(7)	0.3362(7)	1/2					0.43†	0.5 Al
T*	0.2622(5)	0.2057(5)	1/2	0.0008(4)	0.0019(4)	0.012(3)	−0.0002(4)	0.34	0.2 Al
Oab1	0.3591(5)	0.4110(6)	1/2					0.41(2)	0.3 O
Oab2	0.3509(2)	0.4356(2)	1/2					0.41†	0.5 O
Oab*	0.3791(6)	0.4039(7)	1/2					0.41†	0.2 O
Oc	1/2	0	1/2	0.0049(6)	0.0043(6)	0.063(3)	−0.0006(3)	1.42	0.4 O
Oc*	0.4501(5)	0.0502(4)	1/2	0.0021(5)	0.0016(5)	0.029(3)	−0.0003(3)	0.61	0.2 O
Od	0.1188(2)	0.2259(2)	0.024(1)					0.51(2)	0.3 O
Od*	0.1409(2)	0.2067(2)	0.020(2)					0.51†	0.2 O

** In model 1 the refined scattering lengths for T and T* were 0.2933(15)*f* and 0.0726(15)*f*, respectively.
† In model 2 the isotropic temperature factors of the individual positions of a split site were constrained to be equal.

AlO_4 tetrahedra form T_3O groups corresponding to the T^*T_2O groups in mullite. There are no double tetrahedral chains in the $Al_5(BO_3)O_6$ structure because every alternate bridging O site along the **c** axis is vacant, corresponding to $x = 1.0$ in the mullite formula if the B atoms are considered to replace Al in one-quarter of the T sites:

$$Al_2[Al_{2+2x}Si_{2-2x}]O_{10-x}, \quad x = 1.0 \rightarrow Al_2[Al_4]O_9 \rightarrow Al_2[Al_3B]O_9. \quad (5)$$

In the sillimanite structure, the Si and Al sites have slightly different x and y coordinates; therefore, our mullite model includes a splitting of the T site in the plane $xy\frac{1}{2}$ into T1 (0.3 Si) and T2 (0.5 Al). Associated with the ordering of Si and Al in sillimanite are displacements of the coordinating O atoms toward the Si sites. The Oab site in mullite was therefore split into two sites (Oab1 and Oab2) to correspond to Si or Al occupancy of T, and into a third position, Oab* corresponding to occupancy of T*. The situation of the Od site in mullite is more complicated, as it is bonded to two tetrahedral cations, and a number of local configurations are possible: T-Od-T, T-Od-T*, T*-Od-T, and T*-Od-T*. On the basis of the $Al_5(BO_3)O_6$ structure, and because it would require the presence of two adjacent Oc vacancies, we exclude the possibility of T*-Od-T* linkages. Also, in $Al_5(BO_3)O_6$ the O atoms equivalent to Od in mullite are displaced toward the T site and away from the T* sites. Computer simulations of mullite-like defects in sillimanite (Padlewski et al., in preparation) suggest that these same displacements occur within mullite itself. We therefore allocated 0.2 O atoms to an Od* site off the plane $z = 0$ in mullite. The remaining Od sites are assumed to be involved in Al-Od-Si linkages (i.e., T-Od-T), and our analogy with sillimanite suggests that these too should be displaced off the plane $z = 0$.

TABLE 3. Bond lengths for mullite

	Model 1		Model 2	
Al-Oab	[4]	1.8949(3)	Al-Oab1	1.921(3)
			-Oab2	1.899(1)
			-Oab*	1.862(3)
-Od	[2]	1.9356(5)	-Od	1.956(1)
			-Od*	1.914(2)
T-Oab		1.708(1)	T1-Oab1	1.680(9)
-Oc		1.6688(9)	-Oc	1.631(7)
-Oc*		1.729(4)	-Od	1.667(6)
-Oc*		1.783(4)		
-Od	[2]	1.7271(6)	T2-Oab2	1.702(6)
			-Oc	1.696(5)
			-Oc*	1.749(7)
			-Oc*	1.811(6)
			-Od	1.751(5)
			-Od*	1.707(7)
T*-Oab		1.809(4)	T*-Oab	1.761(7)
-Oc*		1.856(5)	-Oc*	1.858(5)
-Od	[2]	1.772(2)	-Od*	1.761(6)

The results from the refinement of this split-site model are reported in Tables 1, 2, and 3 as model 2. Table 4[1] contains calculated and observed structure factors for both models. It is gratifying to note that the refined splittings (e.g., the z coordinates of Od and Od*) are very similar to those found in sillimanite and $Al_5(BO_3)O_6$. Although there is no direct information regarding correlations between the occupancies of various partially occupied sites in this model of mullite, by considering some of the T-O distances (Table 3), it is possible to deduce some of the local arrangements or clusters that probably occur within the crystal. The geometry of these clusters also compares favorably with those found in sillimanite and $Al_5(BO_3)O_6$ (Figs. 2 and 3).

[1] To receive a copy of Table 4, order document AM-91-452 from the Business Office, Mineralogical Society of America, 1130 Seventeenth Street NW, Suite 330, Washington, DC 20036, U.S.A. Please remit $5.00 in advance for the microfiche.

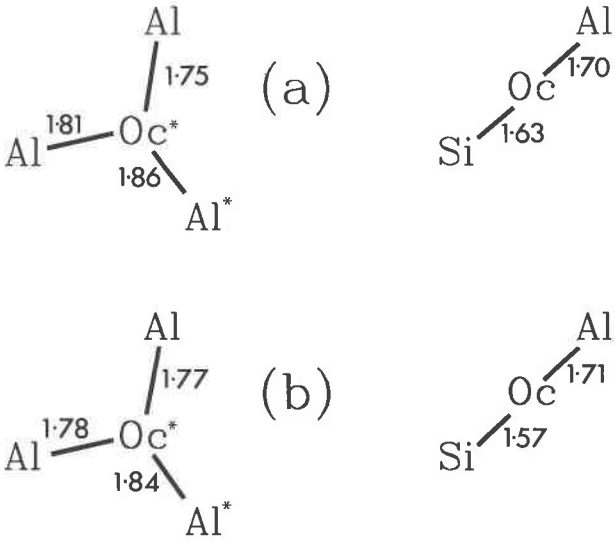

Fig. 2. (**a**) Possible local environments around the Oc site of mullite, derived from the split-site model on the basis of bond lengths (Table 3), compared to (**b**) configurations found in $Al_5(BO_3)O_6$ and sillimanite. Numbers are bond lengths in Å.

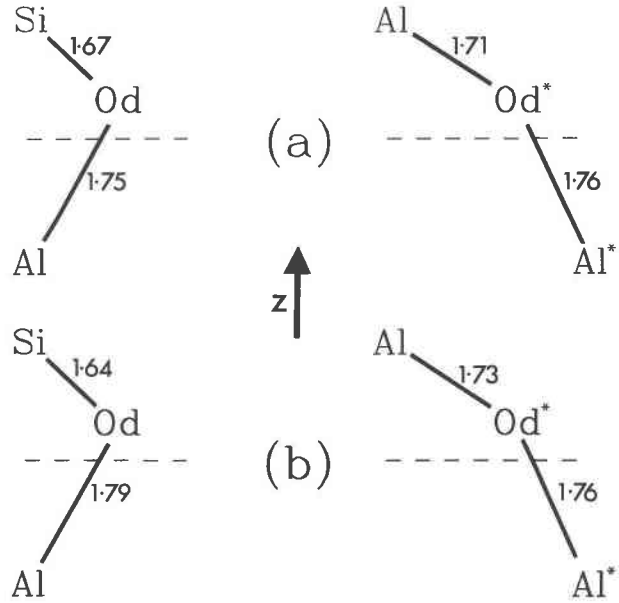

Fig. 3. (**a**) Possible local environments around the Od site of mullite, derived from the split-site model on the basis of bond lengths (Table 3), and compared to (**b**) configurations found in sillimanite and $Al_5(BO_3)O_6$. The dashed line indicates the plane $z = 0$, which is an m_z mirror in the mullite average structure; only one of each of the symmetrically equivalent local configurations is shown in **a**.

Superstructure

The modulated ordering within the mullite structure gives rise to the satellite reflections within the diffraction pattern. Their position, at $\frac{1}{2}\mathbf{c}^* \pm 0.30\mathbf{a}^*$, indicates that the ordering patterns have repeat periods of 2 unit cells along the **c** axis and approximately 3.3 unit cells along the **a** axis. However, the analysis of McConnell and Heine (1984) allows the ordering to be analyzed in terms of two ordering patterns, each with unit cells $a \times b \times 2c$, which then occur successively along the modulation direction. These ordering schemes are represented by the two difference structures $\rho_1(\mathbf{r})$ and $\rho_2(\mathbf{r})$, whose symmetries were determined to be P_cnnm and P_cbnm, respectively, by a combination of group theoretical analysis (McConnell and Heine, 1985a) and experimental results (Angel and Prewitt, 1987). These ordering patterns can, in principle, be refined directly by using the satellite intensities and a superspace group. However, because the satellite reflections are so weak and diffuse (Welberry and Withers, 1990), we derive the ordering schemes from examination of two Patterson functions related to the two ordering patterns. The plus Patterson function (P_+) is simply the sum of the Patterson functions of the two ordering schemes, whereas the minus Patterson function (P_-) is a cross-correlation function between the pair of ordering patterns (McConnell and Heine, 1984). Our analysis, described below, proceeded by postulating two ordering patterns and constructing the corresponding difference structures $\rho_1(\mathbf{r})$ and $\rho_2(\mathbf{r})$. The difference structures $\rho_1'(\mathbf{r})$ and $\rho_2'(\mathbf{r})$ were then derived using Equation 3, and from these we calculated the satellite intensities (Eqs. 4.3 and 4.4 of McConnell and Heine, 1984), from which Patterson functions were then constructed. These calculated Patterson functions were then compared with the two Patterson functions constructed from the observed satellite intensity data (Figs. 4A, 5A). In addition, the calculated satellite intensities were compared with the observed intensities by calculating a conventional R index ($= \Sigma\|F_o| - |F_c\|/\Sigma|F_o|$) for the 264 data with $F_o \geq 3\sigma_F$. Note that these were calculated without any refinement of any structural parameters; only the scale factor was refined.

It is expected from examination of the average structure that a major contribution to the ordering in mullite comes from the arrangement of the O atoms and vacancies on the bridging sites (Oc and Oc*) of the tetrahedral chains, together with the consequent ordering involving T and T* and the displacements of the O atoms on the Oab and Od sites. This ordering is restricted to the P_cnnm [i.e., $\rho_1(\mathbf{r})$] difference structure because ordering on the Oc site is not permitted by the P_cbnm symmetry of $\rho_2(\mathbf{r})$. The absolute magnitude of this O-vacancy ordering is degenerate with the scale factor for the satellite reflections and thus cannot be determined. The assumption was therefore made that these O atoms and vacancies are maximally ordered; the magnitude of this ordering was set to 0.2 atoms overall on the Oc + 2Oc* sites, resulting in maximum and minimum occupancies of 1.0 and 0.6 O atoms. The Patterson maps calculated on this basis (Figs. 4B and 5B) reproduce many of the major features of the Patterson maps calculated from the data (Figs. 4A and 5A), confirming that O-vacancy ordering is a major feature of the incommensurate structure of mullite. Note that, unlike the previous analysis (Angel and Prewitt,

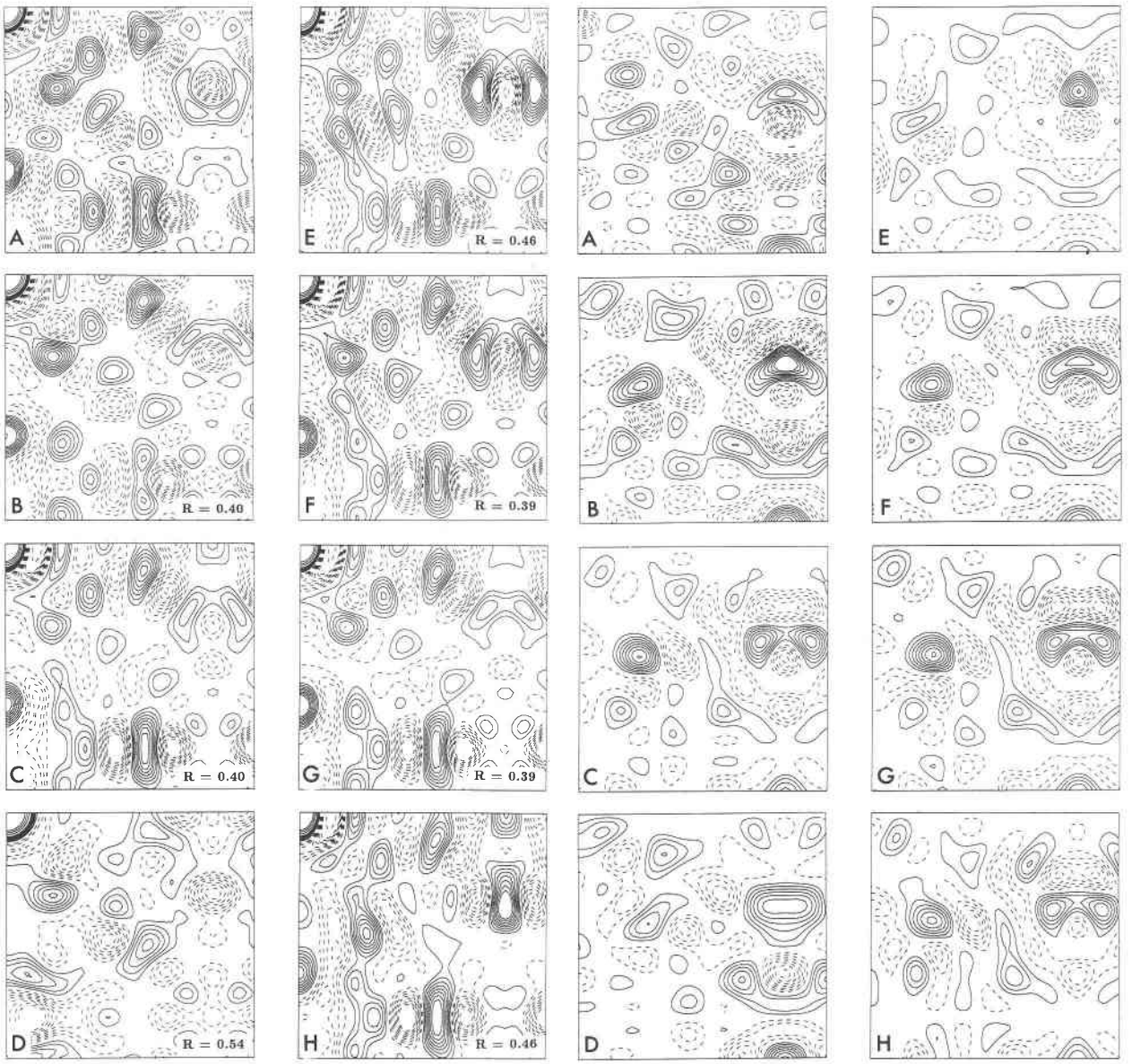

Fig. 4. The (uv0) sections of plus Patterson functions of mullite. (**A**) is constructed from the observed satellite data, (**B**)–(**H**) are calculated from various models described in the text. All maps run from u = 0 to u = 0.6 down the page, and v = 0 to v = 0.6 across the page. The R index calculated for 264 satellites with $F_o \geq 3\sigma_F$ is also given for each model to provide a quantitative comparison among them.

Fig. 5. The (uv0) sections of minus Patterson functions of mullite. (**A**) is constructed from the observed satellite data, (**B**)–(**H**) are calculated from various models described in the text.

1987), the P_ function from this ordering alone (Fig. 5B) is not zero. This is because although $\rho_2(\mathbf{r})$ is identically zero, both of the difference structures used to calculate the P_ Patterson, $\rho_1'(\mathbf{r})$ and $\rho_2'(\mathbf{r})$, are nonzero (Eq. 3). In the regions of the maps most sensitive to the pattern of O displacements within the difference structures, the agreement between calculated and observed Patterson functions is poor. This suggests that additional ordering of Al and Si is present within mullite. Indeed, our interpretation of the average structure (Figs. 2 and 3) implies that at least some of the Al-Si ordering is driven by the ordering of T-T* occupancies. Further maps were therefore calculated from a number of ordering models to test this possibility.

The introduction of Al-Si ordering adds two more variables into the analysis, i.e., the magnitudes of Al-Si ordering (including their signs) in each of the two difference structures. We first consider the addition of Al-Si ordering to the P_cnnm difference structure. If only Al-containing T sites are linked to T* sites, the range of ordering allowed on the fully occupied T site is from $Al_{1.0}$ to $Al_{0.4}Si_{0.6}$, and the corresponding occupancies of the less-

TABLE 5. Site occupancies in mullite component structures

Site	Avg. occ.	$P_c nnm$ Amp.	$+\rho_1(\mathbf{r})$ Occ.	$-\rho_1(\mathbf{r})$ Occ.	$P_c bnm$ Amp.	$+\rho_2(\mathbf{r})$ Occ.	$-\rho_2(\mathbf{r})$ Occ.
T1	0.3 Si	−0.2	0.1	0.5	−0.1	0.2	0.4
T2	0.5 Al	+0.4	0.9	0.1	+0.1	0.6	0.4
T*	0.2 Al	−0.2	0.0	0.4	0.0	0.2	0.2
Oab1	0.3 O	−0.2	0.1	0.5	−0.1	0.2	0.4
Oab2	0.5 O	+0.4	0.9	0.1	+0.1	0.6	0.4
Oab*	0.2 O	−0.2	0.0	0.4	0.0	0.2	0.2
Oc	0.4 O	+0.2	0.6	0.2	0.0	0.4	0.4
Oc*	0.2 O	−0.2	0.0	0.4	0.0	0.2	0.2
Od	0.3 O	−0.2	0.1	0.5	−0.1	0.2	0.4
Od*	0.2 O	+0.2	0.4	0.0	0.0	0.2	0.2

Note: The table lists the average site occupancies for each site in the mullite structure together with the amplitudes and signs of the two ordering patterns of the best-fit model of the incommensurate structure. Together, these define the local occupancies in the component structures $\rho_{ave}(\mathbf{r}) + \rho_1(\mathbf{r})$, etc.

occupied T site are $Si_{0.6}$ and $Al_{0.6}$, respectively. The Patterson functions calculated from these ordering patterns, which also include the relevant O displacements (Figs. 4C, 4D, and 5C, 5D), show that the second of these two extremes is inconsistent with the experimental data. Further calculations show that the magnitude of Al-Si ordering within $P_c nnm$ is not critical to the appearance of the Patterson functions, provided the Al content of the more occupied T site exceeds 0.8. Our subsequent calculations therefore proceeded on the basis of a $P_c nnm$ difference structure containing what we term an optimal degree of Al-Si order; this has $T_{1,0} = Al_{0.9}Si_{0.1}$ and $T_{0,6} = Al_{0.1}Si_{0.5}$, an arrangement that not only meets the criteria derived from examination of the average structure, but also avoids Al-Oc-Al linkages. Patterson functions corresponding to this ordering pattern are shown in Figures 4G and 5G.

Heine and McConnell (1984) showed that an incommensurate modulation in an insulator such as mullite must be stabilized by the gradient interaction of two ordering schemes. The final step in our analysis is therefore to characterize the ordering within the second difference structure, $\rho_2(\mathbf{r})$. Since this has symmetry $P_c bnm$, only Al-Si ordering is allowed, and if we assume that no Si occupies the T* sites, then this ordering must be restricted to the T sites and have the same pattern as that found in sillimanite (McConnell and Heine, 1985a). Again, a continuous range of ordering is possible. As all of the T sites are 80% occupied, occupancy ranging from $Al_{0.8}$ to $Al_{0.2}Si_{0.6}$ is allowed on a particular T site, the occupancies of the remaining sites being constrained by symmetry. Figures 4E–4H and 5E–5H were calculated with varying degrees of order in $P_c bnm$ while retaining the optimal ordering pattern in $P_c nnm$. The pairs of Figures 4E, 5E and 4H, 5H were calculated from maximum ordering in $P_c bnm$, but with opposite signs. This corresponds to changing the order in which the ordering patterns occur along the modulation wave from $+\rho_1(\mathbf{r})$, $+\rho_2(\mathbf{r})$, $-\rho_1(\mathbf{r})$, $-\rho_2(\mathbf{r})$ . . . , to $+\rho_1(\mathbf{r})$, $-\rho_2(\mathbf{r})$, $-\rho_1(\mathbf{r})$, $+\rho_2(\mathbf{r})$ . . . . Comparison of the P_- functions (Figs. 5E, 5H) clearly indicates that the first choice is the correct solution. The series of Patterson functions shown in Figures 4E, 4F, 4G and 5E, 5F, 5G is representative of the effects of decreasing the degree of Al-Si order in $P_c bnm$ from maximum (Figs. 4E, 5E) to zero (Figs. 4G, 5G) through a difference structure that represents the maximum degree of ordering without the necessity of generating any Al-O-Al linkages (Figs. 4F, 5F). This last model, with the site occupancies detailed in Table 5, seems to represent the best match (Figs. 4F, 5F) to the experimental data.

The major discrepancies between the best calculated (Figs. 4F, 5F) and the observed Patterson functions are still in those areas in which the density arises from vectors between the various O sites. Although these generally have the correct sign, they are incorrect in detail. This can be attributed in part to the shortcomings of our description of the O sites in the model of the average structure; for example, even the split-site model for the Oab site still results in T-O bond lengths (Table 3) that are intermediate between those expected for Al-O and Si-O bonds. The split between the true positions of the O atoms in these two environments should therefore be larger, and the contribution to the Patterson functions thereby modified. Similarly, the bridging O site of the tetrahedral chains has been modeled as a central Oc site together with two Oc* sites correlated with the T* site occupancy. However, by analogy with sillimanite, we would expect the bridging O atom of Al-O-Si groups also to be displaced from the symmetry center. Attempts to model such a movement in average structure refinements were unsuccessful because of correlations between parameters, so we were unable to include the effect of such a displacement in our models for the incommensurate ordering.

A physical picture of this ordering in mullite is best obtained by considering unit cells within the crystal where $\mathbf{q}\cdot\mathbf{l} = n\pi/2$. For example, where $\mathbf{q}\cdot\mathbf{l} = 2n\pi$, $\sin(\mathbf{q}\cdot\mathbf{l})$ is zero, $\cos(\mathbf{q}\cdot\mathbf{l})$ is unity, and the structure is given by $\rho_{ave}(\mathbf{r}) + \rho_1(\mathbf{r})$ in Equation 1. Similarly, the second ordering pattern appears in unit cells where $\mathbf{q}\cdot\mathbf{l} = (n + 1)\pi/2$. The structure within the crystal in two such cells is drawn out in Figure 6; these will be referred to as the component structures. It will be noted that both of the component structures contain sites with partial occupancy, indicating

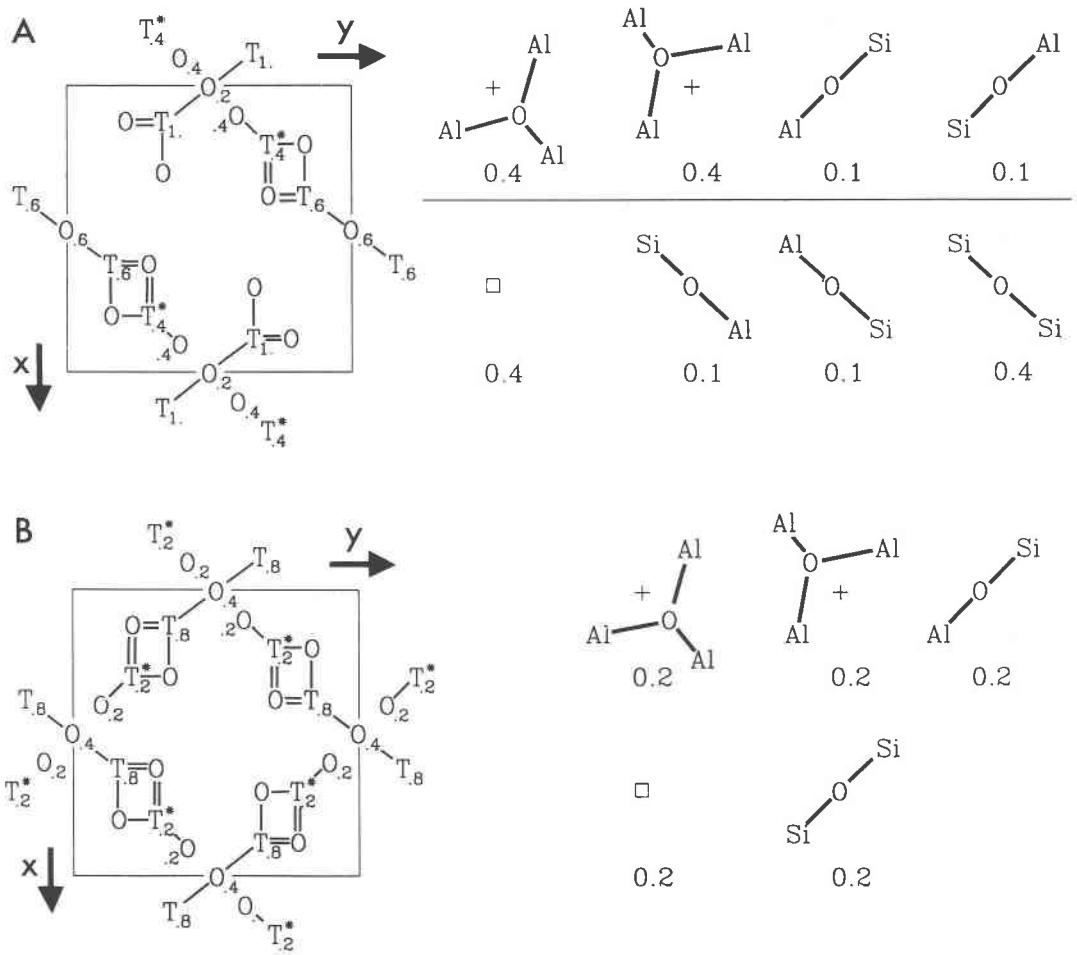

Fig. 6. The (001) layers of the component structures derived from the best fit to the observed satellite intensity data. The O atoms at the Oab and Od sites are included, but their displacements are not shown; details of these and the distribution of Al and Si among the tetrahedral sites of both components are given in Table 5. (**A**) The component structure $[\rho_1(\mathbf{r}) + \rho_{ave}(\mathbf{r})]$ derived from the P_cnnm difference structure exhibits O atom–vacancy ordering and ordering of the overall occupancies of the tetrahedral sites (T and T*) in addition to Al-Si ordering (Table 5). Possible local configurations around the two distinct Oc sites within this component are shown on the right side of the diagram, together with their frequency of occurrence. The + provides an indication of the undisplaced O position Oc, the □ indicates a vacancy. (**B**) The component structure $[\rho_2(\mathbf{r}) + \rho_{ave}(\mathbf{r})]$ derived from the P_cbnm difference structure exhibits Al-Si ordering on the T sites (Table 5) without ordering either O atoms and vacancies on Oc, or the occupancy of T*. The right side illustrates the possible local configurations around the single Oc position in this component.

that, like the average structure, they too are an average. This average is taken over all of the crystal with the same value of $\mathbf{q}\cdot\mathbf{r}$, which in mullite is a (100) plane, perpendicular to the modulation direction. Because of the ½**c*** component of the ordering vector, both component structures also have a two-layer repeat along the **c** axis, with successive layers having the opposite ordering pattern. Thus a site that is enriched in Si in one layer will be enriched in Al in the adjacent layers.

The P_cnnm component structure (Fig. 6A) has maximum ordering of O atoms and vacancies over the bridging O atom positions of the tetrahedral chains, which drives the ordering of Al into the T* sites. This in turn is responsible for the displacement of further O atoms from the Oc position to Oc* and for small movements of the O atoms on the Oab and Od sites. Because of the presence of a symmetry center at the Oc position, the component structure appears to contain a $T_2T_2^*O$ group. Not only is this unreasonable on crystal-chemical grounds, as it would require T*-O bonds of 2.2 Å, but such configurations are specifically excluded by the studies of the diffuse scattering from mullite by Welberry and Withers (1990). This group must therefore represent a centrosymmetric average of two acentric T_2T^*O groups, which we believe to be Al_3O groups like those found in $Al_5(BO_3)O_6$. As illustrated in Figure 6A, this accounts for 80% of the

groups at a fully occupied bridging O atom site; the remainder may be Si-Oc-Al groups. The second type of bridging O atom site in this component is 40% vacant; however, when it is occupied, our best-fit model is consistent with the formation of a mixture of Al-O-Si and Si-O-Si groups.

The P_cbnm component structure (Fig. 6B) contains 20% vacancies on the bridging O atom sites, and symmetry requires that these must be distributed at random, as far as the incommensurate ordering is concerned. Consequently, both of these sites (Oc and Oc*) and the two tetrahedral sites, T and T*, retain the same overall occupancy as the average structure, and the only ordering is that of Al and Si over the T sites following the sillimanite pattern together with associated displacements of the Oab and Od O atoms. As in the P_cnnm component, the T-O-T group in the P_cbnm component represents an average, consisting of Al_3O groups, probably with Si-O-Al and Si-O-Si groups.

Conclusions

We have successfully demonstrated that mullite contains two ordering schemes that are modulated in quadrature along the [100] direction. In addition to confirming the general features of these ordering schemes deduced by Angel and Prewitt (1987), we have identified the presence of Al-Si ordering within both components of the modulation. The degree of ordering most consistent with the experimental data corresponds to an Al-Si distribution that allows the local environments within the mullite crystal to resemble those found in similar stoichiometric and commensurately ordered structures. The driving force for Al-Si ordering appears to be the exclusion of Si from T sites linked to Al-containing T* sites within a $T_2T^*Oc^*$ grouping. Not only is the local charge balance optimized at the Oc* site by this scheme (Sadanaga et al., 1962), but it also explains why **q** is not parallel to **a*** for compositions $x \geq 0.50$; the composition $x = 0.50$ corresponds to the Al-rich limit of this avoidance rule for Si (Ylä-Jääski and Nissen, 1983). Further local ordering of O atoms and vacancies, over and above that represented by the incommensurate modulation, must occur within the structure if $T_2T_2^*Oc$ groups are to be avoided, and this was recently confirmed by an analysis of the diffuse scattering from this same sample of mullite (Welberry and Withers, 1990). Computer simulations by Padlewski et al., (in preparation) of various local configurations in mullite also show that the most energetically favorable arrangement of atoms around an Oc* position is Al_2Al^* and that $T_2T_2^*Oc$ groups can be excluded on the basis of these calculations. The presence of both this short-range order, and the incommensurate order, means that the mullite solid solution is essentially completely ordered with almost zero configurational entropy and a lower enthalpy than a corresponding disordered phase.

We should also emphasize that we have succeeded, as predicted by Simmons and Heine (1987), in interpreting the ordering in mullite with an analysis based upon the physics of ordering at temperatures just below T_c, whereas our data was collected from the crystal at temperatures far below T_c. This analysis has avoided all of the problems associated with refinements of such structures that employ arbitrary supercell methods; by using the plus and minus Patterson functions, we are able to identify the ordering schemes without losing the fundamental incommensurate nature of the structure. It is to be hoped that, in the future, our results will provide the basis for a suitably constrained (Simmons and Heine, 1987) four-dimensional refinement of a diffraction data set measured using mullite exhibiting sharp satellite reflections.

Acknowledgments

We would like to thank Volker Heine and Desmond McConnell for their continuing interest in, and support for, this project. John Hughes and Michael Phillips provided extensive and helpful reviews of the manuscript. The neutron diffraction experiments were performed at the high flux beam reactor at Brookhaven National Laboratory under contract number DE-AC02-76CH00016 with the U.S. Department of Energy and supported by its Office of Basic Energy Sciences. We gratefully acknowledge the support of NATO, the Carnegie Institution of Washington, and the Royal Society in the form of Research Fellowships to R.J.A., as well as NSF grant EAR-8618602 to C.T.P.

References cited

Angel, R.J., and Prewitt, C.T. (1986) Crystal structure of mullite: A reexamination of the average structure. American Mineralogist, 71, 1472–1482.

——— (1987) The incommensurate structure of mullite by Patterson synthesis. Acta Crystallographica, B43, 116–126.

Becker, P.J., and Coppens, P. (1974) Extinction within the limit of validity of the Darwin transfer equations. I. General formalisms for primary and secondary extinction and their application to spherical crystals. Acta Crystallographica, A30, 129–147.

Burnham, C.W. (1964) Crystal structure of mullite. Annual Report of the Director, Geophysical Laboratory, Carnegie Institution of Washington, 63, 223–227.

Cameron, W.E. (1977) Composition and cell dimensions of mullite. American Ceramic Society Bulletin, 56, 1003–1007.

Ďurovič, S. (1969) Refinement of the crystal structure of mullite. Chemicke Zvesti, 23, 113–128.

Ďurovič, S., and Fejdi, P. (1976) Synthesis and crystal structure of germanium mullite and crystallochemical parameters of D-mullites. Silikaty, 20, 97–112.

Finger, L.W., and Prince, E. (1975) A system of FORTRAN-IV computer programs for crystal structure computations. U.S. National Bureau of Standards Technical Note 854.

Fischer, R.X. (1985) STRUPLO84, a FORTRAN plot program for crystal structure illustrations in polyhedral representation. Journal of Applied Crystallography, 18, 258–262.

Grant, D.F., and Gabe, E.J. (1978) The analysis of single-crystal Bragg reflections from profile measurement. Journal of Applied Crystallography, 11, 114–120.

Heine, V., and McConnell, J.D.C. (1984) The origin of incommensurate structures in insulators. Journal of Physics, C17, 1199–1220.

Koester, L., and Steyerl, A. (1977) Neutron physics. In Springer tracts in modern physics, vol. 80. Springer-Verlag, Berlin.

McConnell, J.D.C., and Heine, V. (1984) An aid to the structural analysis of incommensurate phases. Acta Crystallographica, A40, 473–482.

——— (1985a) Incommensurate structure and stability of mullite. Physics Review, B31, 6140–6142.

——— (1985b) The symmetry properties of difference Patterson functions. Acta Crystallographica, A41, 382–386.

Peterson, R.C., and McMullan, R.K. (1986) Neutron diffraction studies of sillimanite. American Mineralogist, 71, 742–745.

Sadanaga, R., Tokonami, M., and Takéuchi, Y. (1962) The structure of mullite, $2Al_2O_3 \cdot SiO_2$, and its relationship with the structures of sillimanite and andalusite. Acta Crystallographica, 15, 65–68.

Simmons, E.H., and Heine, V. (1987) Deriving the two-component description of incommensurate structures from the superspace group. Acta Crystallographica, A43, 626–635.

Sokolova, E.V., Azizov, A.V., Simonov, M.A., Leonyuk, N.I., and Belov, N.V. (1978) Crystal structure of synthetic 3-orthoborate $[Al_5(BO_3)O_6]$. Doklady Akadamii Nauk SSSR, 243, 655–658 (in Russian).

Welberry, T.R., and Withers, R.L. (1990) An optical transform and Monte Carlo study of the diffuse X-ray scattering in mullite, $Al_2(Al_{2+2x}Si_{2-2x})O_{10-x}$. Physics and Chemistry of Minerals, 17, 117–124.

de Wolff, P.M., Janssen, T., and Janner, A. (1981) The superspace groups for incommensurate crystal structures with a one-dimensional modulation. Acta Crystallographica, A37, 625–636.

Ylä-Jääski, J., and Nissen, H.-U. (1983) Investigation of superstructures in mullite by high resolution electron microscopy and electron diffraction. Physics and Chemistry of Minerals, 10, 47–54.

Manuscript received June 11, 1990
Manuscript accepted December 20, 1990